Transport probe of the nonadiabatic transition caused by moving Majorana zero modes

Luting Xu* and Xin-Qi Li†

Center for Joint Quantum Studies and Department of Physics, School of Science, Tianjin University, Tianjin 300072, China

(Received 25 November 2021; revised 22 April 2022; accepted 8 June 2022; published 15 June 2022)

We propose a transport probe scheme to detect the nonadiabatic transition caused by moving Majorana zero modes. The scheme is analyzed theoretically by means of a time-dependent single-electron-wave-function approach to quantum transport. Based on the Kitaev model, we simulate the time-dependent currents and examine the feasibility of using the currents to infer the nonadiabatic transition. In particular, we develop a method to determine the Landau-Zener tunneling ratio in the context of transport, and compare it with the result computed from the same Majorana moving in the isolated quantum wire. Desirable agreements are demonstrated for the whole proposed scheme.

DOI: 10.1103/PhysRevB.105.245410

I. INTRODUCTION

The nonlocal nature of the Majorana zero modes (MZMs) and the intrinsic non-Abelian braiding statistics, both implying immunity from the influence of local environmental noises, promise a sound potential for topological quantum computation [1–6]. The braiding operation is actually exchanging the Majorana modes in real space, which leads to a unitary rotation in the degenerate subspace of ground states. The unitary rotation can constitute desired quantum information processing and realize logic gates in topological quantum computation.

For braiding operations, the early and representative scheme is quantum-adiabatically moving the MZMs by tuning a series of electric gates to drive different regions of the Majorana quantum wire into the topological or nontopological regime [7–10], being guided by the fact that the MZMs will form at the boundaries between the topological and nontopological regions. The subsequent alternative proposals include tuning the couplings between Majorana modes directly or indirectly via modulating the charging energy on the Majorana island or through quantum dots [11–21], measurement-only schemes [22–25], and others [26]. We notice that, with the progress of gating control techniques, the Majorana moving schemes have gained renewed interest in the past years [27–31]. In order to realize the topological protection, i.e., to restrict the quantum evolution in the subspace of the ground states, the quantum moving should be adiabatically slow. However, this may contradict other requirements such as avoiding the quasiparticle-poisoning decoherence. In practice, the adiabatic condition may be violated by finite braiding rates, and the effects of nonadiabatic transition constitute thus an important subject among the studies [27,32–37].

Rather than simulating the nonadiabatic effects in the isolated quantum wires [27,32–37], we raise the question of how to probe the nonadiabatic transition by experimental measurements. This interesting problem, to the best of our knowledge, has not been studied so far in the literature. In this work, we will propose a transport probe scheme to infer the Majorana-moving-caused nonadiabatic transition, as schematically shown in Fig. 1, which is actually the minimal setup of tunneling spectroscopy of Majorana conductances.

Conceptually, as shown in Fig. 1 for the one-lead (two-terminal) transport setup, in the nonsteady state, the current in the left normal-metallic lead ($I_{\rm L}$) is unequal to the Andreev current ($I_{\rm A}$) owing to formation of extra Cooper pairs in the superconductor. Note that increasingly more electrons in the superconductor (owing to formation of extra Cooper pairs and conversion to normal electrons) will flow back to the left lead through the external circuit, forced by the bias voltage (V) in order to maintain the Fermi level of the superconductor unchanged. In particular, the Andreev-reflection (AR) physics tells us that $I_{\rm L}(t) = I_{\rm Le}(t) + I_{\rm Lh}(t)$ and $I_{\rm A}(t) = 2I_{\rm Lh}(t)$, where $I_{\rm Le}(t)$ is the "electron" current for electrons entering to occupy the empty zero-energy bound states (ZEBS) $|0\rangle_{E_0}$, and $I_{\rm Lh}(t)$ is the "hole" current for electrons entering to annihilate the occupied state $|1\rangle_{E_0}$ (to form Cooper pairs). Since the two processes contributing to $I_{\rm Le}(t)$ and $I_{\rm Lh}(t)$ are not simultaneous, we then know that $I_{\rm Le}(t) \neq I_{\rm Lh}(t)$ and $I_{\rm L}(t) \neq I_{\rm A}(t)$, during the transient stage, or in the more general case, when moving the MZMs.

Since the Andreev current is proportional to the occupation probability of the ZEBS, one can thus extract information of the ZEBS occupation from the Andreev current. During Majorana moving, the nonadiabatic transition will reduce the occupation probability of the ZEBS and affect the Andreev current. However, technically, the complexity to handle this problem is twofold. On one aspect, the quantum moving and transport probing are highly time dependent. We are thus required to apply a time-dependent transport theory. In this work, we will apply the single-electron wave function (SEWF) approach [38–41], which is a time-dependent generalization of the stationary S matrix scattering theory. In particular, this approach was recently extended to the context

*xuluting@tju.edu.cn
†xinqi.li@tju.edu.cn

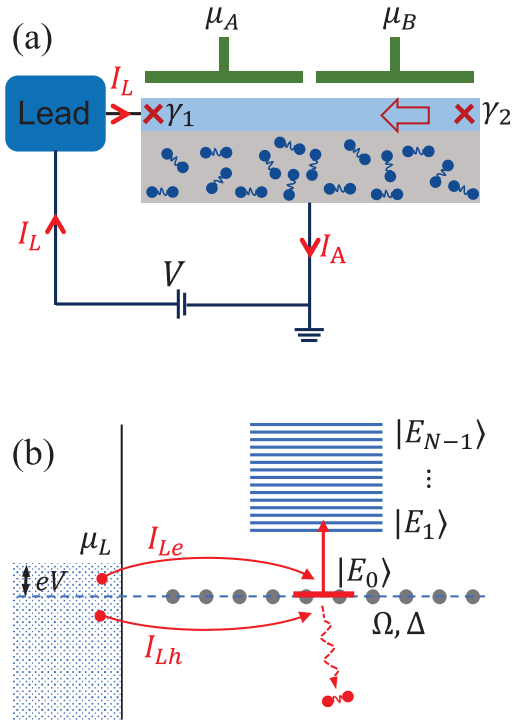

FIG. 1. (a) Schematic setup for transport probe of the nonadiabatic transition caused by Majorana moving, via measuring the time-dependent lead current $I_{\rm L}$ and the Andreev current $I_{\rm A}$ flowing back to the lead from the superconductor through the grounded terminal. The electrochemical potential μ_A is tuned to make the left half wire in the topological regime, while μ_B is changed to make the right half wire from initially topological to finally the nontopological regime. As a consequence, the Majorana mode γ_2 is moved from the right side to the center of the quantum wire. (b) Energy diagram for the transport setup under bias voltage V (with μ_L the chemical potential of the lead). In particular, formation of a Cooper pair by two electrons from the lead through creation and annihilation of the zero-energy (E_0) quasiparticle, and the nonadiabatic transition to the excited states, are schematically shown. The associated "electron" and "hole" currents, $I_{\rm Le}(t)$ and $I_{\rm Lh}(t)$, are also illustrated.

of superconductor-induced Andreev reflections [42]. On the other aspect, determination of the Landau-Zener tunneling ratio is nontrivial in the transport probing process.

The article is organized as follows. We first outline in Sec. II the SEWF approach, in contact with the Kitaev lattice model. Then, in terms of the time-dependent AR coefficient, we display in Sec. III the Andreev currents in three stages and discuss several remarkable features. After carrying out a self-consistency examination, in Sec. IV the Landau-Zener transition ratio properly determined from transport probe is compared with the result calculated in the isolated quantum wire. Full agreement is demonstrated, which is also followed by support from the whole moving-period transition and under (small) finite bias voltages. Finally, we summarize the work in Sec. V with discussions.

II. SINGLE-ELECTRON-WAVE-FUNCTION APPROACH

For the transport setup schematically shown in Fig. 1, the total Hamiltonian can be split into three parts, $H = H_W + H_{\rm lead} + H'$, i.e., the sum of the Hamiltonians of the quantum wire, the transport lead, and their coupling. The Hamiltonian of the transport lead can be simply described by $H_{\rm lead} = \sum_l \epsilon_l a_l^\dagger a_l$, with $a_l^\dagger$ (a_l) the creation (annihilation) operator of the lead electron with energy ϵ_l. In this work, we use l to label the continuum of the lead electron states. The tunnel-coupling Hamiltonian between the quantum wire and the lead is described by $H' = \sum_l t_l c_1^\dagger a_l + {\rm H.c.}$, where $c_1^\dagger$ is the electron operator of the leftmost site of the quantum wire coupling to the lead. Without loss of essential physics, we employ in this work the Kitaev model (spinless p-wave superconductor) to describe the quantum wire. For the s-wave superconductor proximitized Rashba nanowire, one can follow the same treatment developed in this work. The one-dimensional Kitaev lattice model reads as [1]

$$H_W = \sum_j \left[-\mu_j c_j^\dagger c_j - \frac{\Omega}{2}(c_j^\dagger c_{j+1} + {\rm H.c.}) \right] + \frac{\Delta}{2}\sum_j (c_j c_{j+1} + {\rm H.c.}). \quad (1)$$

μ_j is the chemical potential which can be tuned via electric gates, Δ is the order parameter of the superconductor, and Ω is the hopping energy between the nearest-neighbor sites with $c_j^\dagger$ (c_j) the associated electron creation (annihilation) operators. Introducing the Nambu operator $\hat\Psi = (c_1, \ldots, c_N, c_1^\dagger, \ldots, c_N^\dagger)^T$, the Hamiltonian of the quantum wire can be rewritten as $H_W = \frac{1}{2}\hat\Psi^\dagger \widetilde{H}_W \hat\Psi$, with $\widetilde{H}_W$ the well-known Bogoliubov–de Gennes (BdG) Hamiltonian matrix which gives directly the energy spectrum of the Bogoliubov quasiparticles after diagonalization [42]. Instead of the operators basis, the BdG Hamiltonian matrix can be understood as well as constructed under the single-particle state basis $\{|e_1\rangle, \ldots, |e_N\rangle;\ |h_1\rangle, \ldots, |h_N\rangle\}$, where $|e_j\rangle$ and $|h_j\rangle$ describe, respectively, the electron and hole states on the jth site of the quantum wire. Using the electron and hole basis states, the tunnel-coupling Hamiltonian can be rewritten as

$$H' = \sum_l t_l (|e_1\rangle\langle e_l| - |h_1\rangle\langle h_l|) + {\rm H.c.} \quad (2)$$

Here, in order to account for the AR process, we have introduced also the electron and hole states $\{|e_l\rangle, |h_l\rangle\}$ for the transport lead.

Following the single-particle S matrix scattering approach within the Landauer-Büttiker formalism, we notice that an electron entering the superconductor will either excite a Bogoliubov quasiparticle or destroy it, depending on whether the quasiparticle state is empty or occupied. The former case corresponds to the normal tunneling process and the latter results in the Andreev reflection. After accounting for this physics, the tunnel-coupling Hamiltonian is truncated as [42]

$$H' = \sum_l t_l (|\tilde e_1\rangle\langle e_l| - |\tilde h_1\rangle\langle h_l|) + {\rm H.c.}, \quad (3)$$

where the edge states $|e_1\rangle$ and $|h_1\rangle$ are projected onto the subspace of the Bogoliubov quasiparticle states through $|\tilde e_1\rangle = \hat P|e_1\rangle$ and $|\tilde h_1\rangle = \hat P|h_1\rangle$. The projection operator is given by $\hat P = \sum_n' |E_n\rangle\langle E_n|$, with the sum ranging over all the eigenstates of the particle sector of the BdG Hamiltonian matrix.

In this work, we would like to employ the single-electron wave function (SEWF) approach [38–42] for the highly time-dependent transport problem under study, which is actually a time-dependent generalization of the stationary S matrix scattering theory. The basic idea of the SEWF approach is keeping track of the quantum evolution of a single electron initially in the lead, and computing the time-dependent transport coefficients. Let us assume the electron initially in the lead state $|\Psi(0)\rangle = |e_{\bar{l}}\rangle$, and with the incident energy $E_{in} = E_{\bar{l}}$. The subsequent evolution with time will result in a quantum superposition of all basis states of the lead and the quantum wire, as

$$\begin{aligned}|\Psi_{\bar{l}}(t)\rangle &= |\Psi_w(t)\rangle + |\Psi_{\rm leads}(t)\rangle \\ &= \sum_{j=1}^{N}[b_{je}(t)|e_j\rangle + b_{jh}(t)|h_j\rangle] \\ &\quad + \sum_l [\beta_l(t)|e_l\rangle + \tilde{\beta}_l(t)|h_l\rangle]. \end{aligned} \tag{4}$$

Substituting it into the time-dependent Schrödinger equation $i\hbar|\dot{\Psi}\rangle = H|\Psi\rangle$ and applying the technique of Laplace and inverse-Laplace transformations to eliminate the degrees of freedom of the lead, after some algebra, we obtain the equations for the quantum wire state as [42]

$$i\hbar\begin{bmatrix}\dot{b}_{1e}\\ \dot{b}_{2e}\\ \vdots\\ \dot{b}_{Ne}\\ \dot{b}_{1h}\\ \dot{b}_{2h}\\ \vdots\\ \dot{b}_{Nh}\end{bmatrix} = [\widetilde{H}_W + (\hat{P}\Sigma\hat{P})]\begin{bmatrix}b_{1e}\\ b_{2e}\\ \vdots\\ b_{Ne}\\ b_{1h}\\ b_{2h}\\ \vdots\\ b_{Nh}\end{bmatrix} + t_L e^{-\frac{i}{\hbar}E_{\rm in}t}\hat{P}\begin{bmatrix}1\\0\\0\\0\\ \vdots\\ 0\\0\\0\\0\end{bmatrix}. \tag{5}$$

Here we have introduced the self-energy operator

$$\Sigma = (-i\Gamma_L/2)\,(|e_1\rangle\langle e_1| + |h_1\rangle\langle h_1|). \tag{6}$$

The tunnel-coupling rate under the wideband limit reads as $\Gamma_L = 2\pi\rho_L t_L^2$, with ρ_L the density of states of the transport lead, and t_L the constant tunnel-coupling strength (i.e., $t_l = t_L$).

The single ($\bar{l}$) electron currents are obtained through the changing rates of the occupation probabilities of the lead electron and hole, given by

$$\begin{aligned} i_{\rm Le} &= -\frac{e}{\hbar}\frac{\partial P_{\rm Le}}{\partial t} = -\frac{e}{\hbar}\frac{\partial \sum_l |\beta_l(t)|^2}{\partial t}, \\ i_{\rm Lh} &= \frac{e}{\hbar}\frac{\partial P_{\rm Lh}}{\partial t} = \frac{e}{\hbar}\frac{\partial \sum_l |\tilde{\beta}_l(t)|^2}{\partial t}. \end{aligned} \tag{7}$$

One may note that $i_{\rm Le}$ and $i_{\rm Lh}$ are, respectively, the electron and hole currents flowing through the tunnel junction from the lead to the quantum wire. Moreover, after some algebra, one can further obtain

$$\begin{aligned} i_{\rm Le} &= -\frac{e}{\hbar}\left[2t_L{\rm Im}\left(e^{\frac{i}{\hbar}E_{in}t}\langle e_1|\hat{P}|\Psi_w\rangle\right) + \Gamma_L\,|\langle e_1|\hat{P}|\Psi_w\rangle|^2\right], \\ i_{\rm Lh} &= \frac{e}{\hbar}\Gamma_L\,|\langle h_1|\hat{P}|\Psi_w\rangle|^2. \end{aligned} \tag{8}$$

We are thus allowed for very convenient computation for the time-dependent currents by solving Eq. (5) for the time-dependent state $|\Psi_w(t)\rangle$ of the quantum wire.

Along the same line of the Landauer-Büttiker formalism of single-particle scattering theory, the time-dependent currents under finite bias voltage (at zero temperature) can be computed as

$$\begin{aligned} I_{\rm Le} &= \int_{-\mu_L}^{\mu_L} dE_{\bar{l}}\rho_L i_{\rm Le} = \frac{e}{h}\int_{-\mu_L}^{\mu_L} dE_{\bar{l}}\mathcal{T}_L, \\ I_{\rm Lh} &= \int_{-\mu_L}^{\mu_L} dE_{\bar{l}}\rho_L i_{\rm Lh} = \frac{e}{h}\int_{-\mu_L}^{\mu_L} dE_{\bar{l}}\mathcal{T}_A. \end{aligned} \tag{9}$$

Here, we have related the results from the single-particle currents with the conventional theory in terms of transmission coefficients. However, the present SEWF approach is a time-dependent generalization of the Landauer-Büttiker S matrix scattering theory and also of the nonequilibrium Green's function treatment. Note also that the total lead current flowing through the tunnel junction from the lead to the quantum wire is the sum of the electron and hole currents, i.e., $I_{\rm L} = I_{\rm Le} + I_{\rm Lh}$, while the Andreev current flowing back to the transport lead from the quantum wire through the grounded terminal is $I_{\rm A} = 2I_{\rm Lh}$. Accordingly, the linear Andreev differential conductance is given by $G_A = (2e^2/h)\mathcal{T}_A$. The Andreev reflection coefficient $\mathcal{T}_A$ can be calculated through

$$\mathcal{T}_A = \frac{h}{e}\rho_L i_{\rm Lh} = \frac{\Gamma_L^2}{t_L^2}\,|\langle h_1|\hat{P}|\Psi_w\rangle|^2. \tag{10}$$

One can prove that, in steady state, this result will recover the standard expression in terms of the nonequilibrium Green's functions [42].

III. TIME-DEPENDENT CURRENT AND SELF-CONSISTENCY EXAMINATION

The time-dependent SEWF approach outlined above is in particular suitable for simulating the transport probe of nonadiabatic transitions [27,32–37]. In this work, we consider the simplest piano-key model analyzed in Ref. [27]. Let us denote the electrochemical potentials of the left and right half wire by μ_A and μ_B. By fixing μ_A with a value smaller than Ω, the left half is kept in the topological regime, and the right half is tuned according to [27]

$$\mu_B(t) = [1 - f(t/\tau)]\mu_{Bi} + f(t/\tau)\mu_{Bf}, \tag{11}$$

where the initial value of μ_B is set as $\mu_{Bi} = \mu_A$ and the final value μ_{Bf} is larger than Ω. In general, $f(s)$ can be a monotonically increasing function with $f(0) = 0$ and $f(1) = 1$. As an example, one can choose $f(s) = \sin^2(s\pi/2)$. Therefore, the right half of the quantum wire begins in a topological regime with $\mu_{Bi} = \mu_A < \Omega$, and finishes at time τ with $\mu_{Bf} > \Omega$, which drives the right half wire into a trivial regime. As the consequence, the Majorana bound state at the right end of the wire will be moved to the center.

As a preliminary illustration, we display in Fig. 2 the time-dependent behaviors of the Andreev current (in terms of the time-dependent AR coefficient $\mathcal{T}_A$) associated with three stages: (i) steady-state formation of the ZEBS occupation before switching on the gate (μ_B) control for Majorana moving;

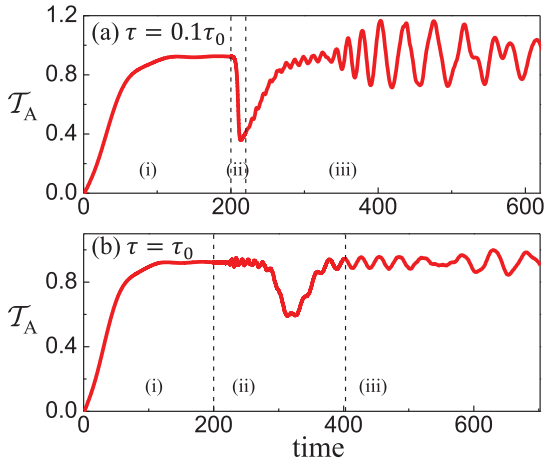

FIG. 2. Time-dependent behaviors of the Andreev reflection current (in terms of the time-dependent AR coefficient $\mathcal{T}_A$) associated with three stages: (i) steady-state formation of the ZEBS occupation before switching on the gate voltage (μ_B) control for Majorana moving; (ii) gate-control Majorana moving; and (iii) after the moving. In the simulation, we set the nearest-neighbor hopping energy $\Omega = 1$ as the energy unit in an arbitrary system of units. Accordingly, other parameters are set as $\Delta = 0.5$, $\mu_A = 0.9$, $\mu_B = (0.9, 1.1)$, $\Gamma_L = 1.0$, and $E_{in} = 0.0$. The moving times are chosen as $\tau = 0.1\tau_0$ in (a) and $\tau = \tau_0$ in (b), while the Landau-Zener characteristic time τ_0 is determined by Eq. (12) in the main text, which gives $\tau_0 = 202.64$.

(ii) gate-control Majorana moving; and (iii) after the moving. In Fig. 2, we first illustrate the gradual formation of steady-state current during stage (i), which indicates the formation of stationary ZEBS occupation. The formation of steady-state current starting with a single $\bar{l}$-lead-electron is somehow a bit tricky. In a simple way, we can say that it corresponds to the long-time limit of the S matrix scattering approach. As a more detailed inspection, in Eq. (5) the initial condition with the $\bar{l}$ electron injection manifests as a driving term, which will result in nonzero occupation of the wire states and nonvanishing continuous current, even in long-time limit. This interesting feature differs from the alternative initial condition by considering the electron initially in the quantum wire, e.g., on the zero-energy bound state, which will unavoidably lose the electron into the continuum of the lead reservoir. This issue can be understood better in the simpler transport problem by considering an electron transmitting through a resonant level of the quantum dot [41]. After a careful check, one can find that the single $\bar{l}$ electron current is extremely small, by noting that the coupling (energy) amplitude [t_l in Eq. (2)] is infinitesimally small, because of the infinite extension of the lead electron wave function in the continuum of eigenstates representation. Therefore, only after multiplying the density of states of the lead, which is infinity for a continuum, the finite result of the current or the transmission coefficient as shown in Eq. (10) can be obtained. We can thus conclude that the steady-state single $\bar{l}$ electron current, which is infinitesimally small and flows for an infinitely long time, does not contradict any physical principle. After multiplying the density of states of the lead and integrating over some energy range, the single electron transmission approach matches well the transport problem under bias voltage, where the external circuit will help to maintain the continuous transport current.

In Fig. 2, for the time-dependent AR coefficient $\mathcal{T}_A$, during the stage (i) discussed above, one may notice that its steady-state value is not ideally quantized to unity. Actually, in the low-energy effective description, the AR coefficient of unity associated with the MZMs is obtained after the higher energy excited states are gapped out from the transport. In our simulation based on the full lattice model, for the purpose of saving simulation time, we have set a relatively strong coupling rate $\Gamma_L = 1.0$. Under this choice, the excited states of the Majorana wire are not fully gapped out during the transport process, thus leading to the quantization of the AR coefficient slightly lower than unity. We have checked that using a weaker coupling rate (smaller Γ_L) can perfectly restore the ideal quantization value.

During the stage (ii) as shown in Fig. 2, modulating μ_B from μ_{Bi} to μ_{Bf} according to Eq. (11) moves the Majorana bound state γ_2 from the right end to the center of the quantum wire. Two moving times, $\tau = 0.1\tau_0$ and τ_0, are chosen for the simulation. Here, the characteristic time τ_0 is determined from the Landau-Zener tunneling analysis [27], which reads

$$\tau_0 = |\mu_{Bf} - \mu_{Bi}| \left(\frac{N_{\text{right}}}{\pi \Delta} \right)^2, \tag{12}$$

with N_{right} the lattice number of the right half wire. Notice that, during the continuous modulation of μ_B, the superconductor energy gap will almost close at $\mu_B = \Omega$ and reopen after $\mu_B > \Omega$. The closing and reopening of the energy gap is associated with a topological phase transition. Accordingly, the nonadiabatic transition is expected to take place mainly when crossing the phase transition point. In Fig. 2(a), for the fast moving with $\tau = 0.1\tau_0$, after crossing the phase transition point, the short time does not allow obvious reoccupation of the ZEBS from injection of the lead electron, resulting thus in the decreasing Andreev current as observed. In contrast, in Fig. 2(b), the slower moving (with $\tau = \tau_0$) reveals a reoccupation behavior after crossing the phase transition point, as indicated by the turnover behavior of the current.

In Fig. 2, we also show the current behavior in stage (iii) after the moving. In this context, we notice two interesting features. One is the current oscillation, which becomes stronger after the fast moving; another is that the AR coefficient $\mathcal{T}_A$ can be larger than 1. The reason for the former is that the occupation of the excited quasiparticle states caused by the nonadiabatic transition will interfere with the reoccupation of the ZEBS owing to new injection, since the AR current is extracted from the left-end site of the quantum wire, which is commonly shared by the ZEBS and the exited states. The occupation of the excited quasiparticle states is also the reason for the second phenomenon mentioned above. This corresponds to an increase of transport channels. From the Landauer-Büttiker scattering theory (the multichannel version), we know that the transport coefficient can be larger than 1.

In the SEWF approach, the net accumulation of the normal tunneling current i_{Le} and the Andreev process current i_{Lh} should correspond to the change of the occupation probability of the ZEBS plus the transition to other excited states. Thus

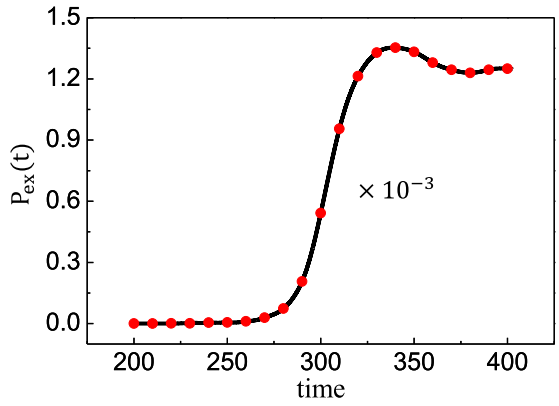

FIG. 3. Self-consistency examination for the total probability of transition to the excited states, with the result of the black line computed through Eq. (13), and the result of the red dots from Eq. (14) based on tracking the wave function of the quantum wire during the transport process. The multiplying factor 10^{-3} inside the figure indicates rescaling the vertical coordinates. Here we consider the contribution of multiple electrons near the incident energy E_{in}, within a small energy window $\Delta E = \alpha\widetilde{\Gamma}_L$ by setting $\alpha = 10^{-2}$, while $\widetilde{\Gamma}_L$ is the tunnel-coupling rate (widening width) of the ZEBS. $\widetilde{\Gamma}_L$ can be determined as $\widetilde{\Gamma}_L = |u_1|^2\Gamma_L$, with u_1 the electron amplitude of the first lattice site (coupled to the lead) in the wave function of the ZEBS, which can be obtained by diagonalizing the BdG Hamiltonian of the quantum wire. All the parameters used here are the same as in Fig. 2.

we have

$$\frac{1}{e}\int_{t_i}^{t}[i_{\rm Le}(t') - i_{\rm Lh}(t')]dt' = [P_{\rm E_0}(t) - P_i] + P_{\rm ex}(t). \quad (13)$$

Here P_i is the initial occupation probability of the ZEBS. In the numerical simulation, we can compute $P_{\rm E_0}(t)$ as $P_{\rm E_0}(t) = |\langle E_0|\Psi_w(t)\rangle|^2$, and $P_{\rm ex}(t)$ as

$$P_{\rm ex}(t) = \sum_j [|\langle E_j(t)|\Psi_w(t)\rangle|^2 + |\langle -E_j(t)|\Psi_w(t)\rangle|^2] - P_{\rm E_0}(t), \quad (14)$$

where the summation is over all the instant eigenstates of the BdG Hamiltonian matrix. As an examination for self-consistency, we compare in Fig. 3 the probability $P_{\rm ex}(t)$ computed through Eq. (14) and the result from Eq. (13). Notice that, as explained above, the currents and the occupation probabilities from a single $\bar{l}$ electron on the two sides of Eq. (13) are infinitesimally small. In the plot of Fig. 3, we consider the contribution of multiple electrons near the energy $E_{\bar{l}}$ of the $\bar{l}$ electron, within a small energy window $\Delta E = \alpha\widetilde{\Gamma}_L$ by setting $\alpha = 10^{-2}$, while $\widetilde{\Gamma}_L$ is the tunnel-coupling rate (widening width) of the ZEBS. Note also that in the numerical simulation we set $\Gamma_L = 2\pi\rho_L|t_L|^2 = 1$. The full agreement in Fig. 3 indicates that we can employ the currents and their accumulations to infer the Majorana-moving-caused nonadiabatic transition, to be analyzed below in detail.

IV. LANDAU-ZENER RATIO INFERRED BY TRANSPORT PROBE

We may regard the Majorana-moving-caused nonadiabatic transition as the Landau-Zener tunneling. For an isolated quantum wire, if we know the initial and final occupation probabilities of the ZEBS, P_i and P_f, we can unambiguously define the Landau-Zener transition ratio as $\gamma = \Delta P/P_i$, where $\Delta P = P_i - P_f$, since this loss of the occupation probability is owing to the nonadiabatic transition. However, for the transport probing, the problem is more complicated. After the first stage, i.e., stage (i) as shown in Fig. 2, steady-state occupation of the ZEBS is achieved. Then, in stage (ii), during the time period (t_i, t) (with $t < t_f$ and $\tau = t_f - t_i$), net accumulation of the quasiparticle-states occupation is the difference of the normal electron injection and the AR loss, while both are given by

$$a = \frac{1}{e}\int_{t_i}^{t} dt'\, i_{\rm Le}(t'),$$
$$b = \frac{1}{e}\int_{t_i}^{t} dt'\, i_{\rm Lh}(t'). \quad (15)$$

We may thus introduce $\widetilde{P}_i = P_i + (a - b)$ and use it to replace P_i, for the "initial" occupation probability on the ZEBS. However, for moving after crossing the phase transition point, the net accumulation is largely not participating in the nonadiabatic transition, owing to the reopening energy gap during the later half time period $(t_i + \tau/2, t_f)$. This insight suggests us to introduce

$$\tilde{a} = \frac{1}{e}\int_{t_i}^{t_i+\tau/2} dt'\, i_{\rm Le}(t'),$$
$$\tilde{b} = \frac{1}{e}\int_{t_i}^{t_i+\tau/2} dt'\, i_{\rm Lh}(t'), \quad (16)$$

to replace the quantities a and b in $\widetilde{P}_i$ after crossing the phase transition point. That is, when $t > t_i + \tau/2$, we use $\widetilde{P}_i = P_i + (\tilde{a} - \tilde{b})$. For all, we define the Landau-Zener transition ratio $\widetilde{\gamma}$ as

$$\widetilde{\gamma} = \frac{\Delta\widetilde{P}}{\widetilde{P}_i}, \quad (17)$$

where the transition probability is given by $\Delta\widetilde{P} = (P_i - P_f) + (a - b)$. Note that here the "final" occupation probability P_f is defined at the running time t.

In Fig. 4, we display the numerical results of $\widetilde{\gamma}$ versus γ for different moving speeds and find desirable agreements. In the numerical simulation, we determine P_i and P_f from the wavefunction of the quantum wire by solving Eq. (5). In practice, they should be extracted from the Andreev current $i_{\rm A}(t) \simeq (2e)\widetilde{\Gamma}_L P_{\rm E_0}(t)$, where $\widetilde{\Gamma}_L$ is the coupling rate of the ZEBS to the lead and the current is recorded by applying a small bias voltage (in the linear response regime). In this extracting protocol, P_i can be determined rather precisely, since there is no nonadiabatic transition to the excited states until the formation of steady state. $P_f(t)$ is expected also to be determined with reasonable precision from $i_{\rm A}(t)$, provided that $\widetilde{\Gamma}_L$ is much smaller than the energy gap and the quantum moving is not so fast.

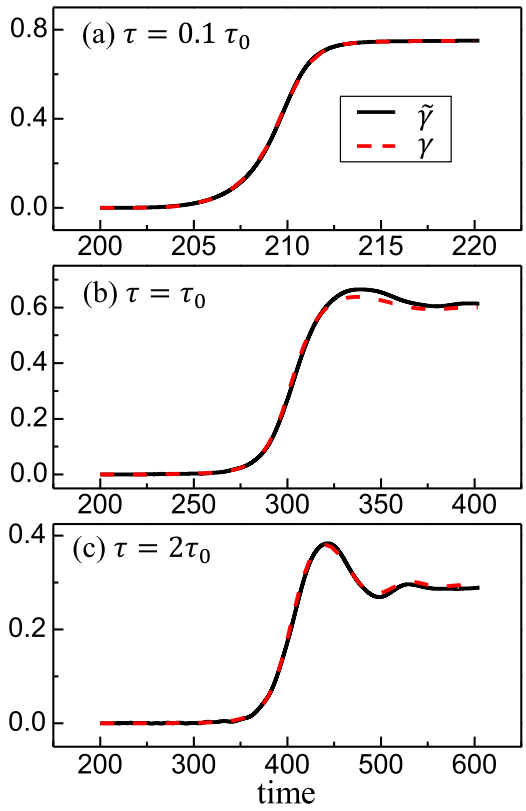

FIG. 4. Landau-Zener transition ratio during the moving process, in comparison between $\tilde{\gamma}$ (inferred by transport probe) and γ (calculated for the isolated quantum wire). Moving times of $\tau = 0.1\tau_0$, τ_0, and $2\tau_0$ are considered, respectively, in (a), (b), and (c). Other parameters are the same as in Fig. 2.

We have shown in Fig. 4 the transient transition behavior during the moving process. Now we further show in Fig. 5 the final result of transition after the entire τ-period quantum moving, which corresponds to the standard characterization of the Landau-Zener tunneling. It is well known that the Landau-Zener tunneling formula predicts exponential dependence on the moving time τ. We see here that, in addition to the good agreement between $\tilde{\gamma}$ and γ, the exponential dependence behavior maintains well for wide range of τ, despite that the present problem is beyond the simple two-level system considered when deriving the Landau-Zener formula. We notice certain deviation only for fast moving (small τ), which is reasonable by noting that, in the limit of $\tau \to 0$, the "transition" is actually from a transformation of the basis states that does not obey the Landau-Zener transition formula.

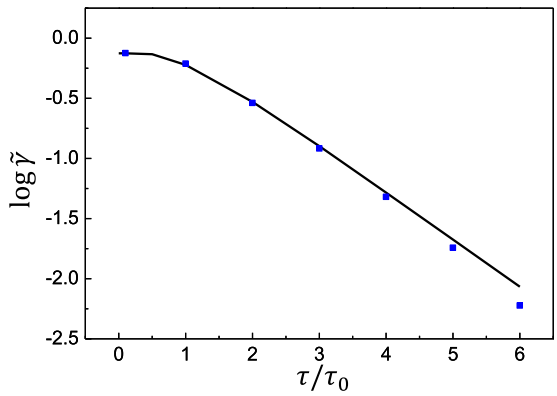

FIG. 5. Landau-Zener transition ratio as a function of the moving time (τ). The results plotted by the filled squares are the ratio $\tilde{\gamma}$ inferred by transport probe, which are compared with the results (solid line) calculated for the isolated quantum wire. Parameters are the same as in Fig. 2.

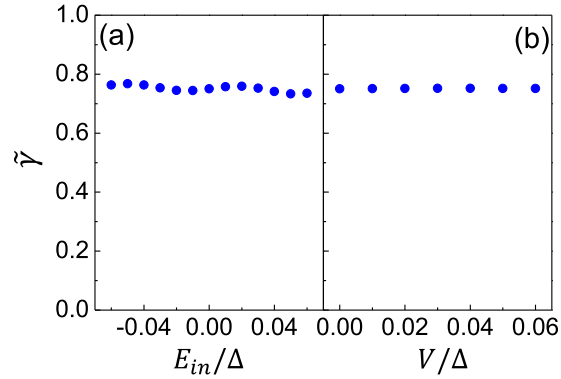

FIG. 6. (a) Landau-Zener transition ratio probed by electrons with different incident energies. (b) Averaged transition ratio for transport probe under (small) finite bias voltages. In this plot we consider the moving time $\tau = 0.1\tau_0$. Other parameters are the same as in Fig. 2.

As explained previously, the single-electron approach can account well for the contribution of multiple electrons at the incident energy $E_{in} = E_{\bar{l}}$, by multiplying a proper constant (the lead electron numbers at this energy). We can thus apply the SEWF approach to compute the differential conductance, which is directly related to the transmission coefficient at zero temperature, and/or compute the linear response current. In practice, one may apply some finite (but also small) bias voltage. In this case, we expect the transport-probe protocol discussed in this work to be valid as well. Indeed, in Fig. 6(a), we show the transition results probed by electrons with different incident energies. And, in Fig. 6(b), we average the results to obtain the transition ratio, which corresponds to the transport probe under different bias voltages. The result is found insensitive to the (small) bias voltages. This observation can benefit the feasibility of the proposed transport probing scheme.

V. SUMMARY AND DISCUSSION

We proposed a scheme to probe the Majorana-moving-caused nonadiabatic effects. Our analysis was based on a recently developed single-electron-wave-function approach, which generalizes the stationary BdG S matrix scattering theory to a time-dependent transport version, being thus in particular suitable for the proposed highly time-dependent transport problem. Via numerical simulation with the Kitaev model, we displayed and discussed the time-dependent behaviors of the Andreev currents flowing back to the lead through the grounded terminal of the superconductor, during the process of Majorana moving. We further examined the feasibility

of using the current to infer the nonadiabatic transition and designed a scheme to determine the Landau-Zener tunneling ratio in the context of transport. By comparing with the results of isolated quantum wire, we demonstrated desirable agreements for both the transient and final Landau-Zener tunneling ratios, together also with simulations under (small) finite bias voltages.

Majorana moving and the nonadiabatic effects are crucial ingredients of braiding dynamics. Understanding the moving effects on Majorana bound states and quasiparticle excitations is a prerequisite for Majorana manipulation with high fidelity, since the manipulation at finite timescales will cause both decoherence and renormalization effects. An important extension of the present study is to consider the typical realization of the Rashba semiconductor nanowire in proximity to an *s*-wave superconductor, while the Kitaev model simulated in this work can be regarded as the strong magnetic field limit. For such more complicated quantum wires, the Landau-Zener characteristic time τ_0 may exhibit significant uncertainty compared with estimated values and may have $1 \sim 2$ orders of magnitude change with the system parameters [27]. Moreover, in realistic quantum wires, Majorana moving passing through static impurities/disorders present in the system may have an essential influence on the nonadiabatic transitions, as qualitatively discussed in Refs. [33,34]. Including such complexities in our time-dependent lattice-model based scheme of simulations should be straightforward. However, further inclusion of inelastic scattering effects, quasiparticle excitation, and poisoning is important but more challenging for theoretical simulations. In this work, we only considered the simplest moving scheme analyzed in Ref. [27]. It will be valuable to simulate the transport probe of nonadiabatic effects associated with other moving schemes, e.g., the domain-wall moving [33,34] and the optimal control of quantum moving to suppress the nonadiabatic transition [35]. Important issues associated with large moving speed may include the stability of the Majorana bound states and possible relativistic effects [33,34]. Simulating all these effects in connection with the transport probe is of great interest for future studies.

ACKNOWLEDGMENTS

This work was supported by the National Key Research and Development Program of China (Grant No. 2017YFA0303304) and the NNSF of China (Grants No. 11675016, No. 11974011, and No. 11904261).

[1] A. Y. Kitaev, Unpaired Majorana fermions in quantum wires, Phys. Usp. **44**, 131 (2001).
[2] A. Y. Kitaev, Fault-tolerant quantum computation by anyons, Ann. Phys. **303**, 2 (2003).
[3] C. Nayak, S. H. Simon, A. Stern, M. Freedman, and S. D. Sarma, Non-Abelian anyons and topological quantum computation, Rev. Mod. Phys. **80**, 1083 (2008).
[4] B. M. Terhal, Quantum error correction for quantum memories, Rev. Mod. Phys. **87**, 307 (2015).
[5] S. D. Sarma, M. Freedman, and C. Nayak, Majorana zero modes and topological quantum computation, npj Quantum Inf. **1**, 15001 (2015).
[6] Y. Oreg and F. von Oppen, Majorana zero modes in networks of Cooper-pair boxes: Topologically ordered states and topological quantum computation, Annu. Rev. Condens. Matter Phys. **11**, 397 (2020).
[7] J. Alicea, Y. Oreg, G. Refael, F. von Oppen, and M. Fisher, Non-Abelian statistics and topological quantum information processing in 1D wire networks, Nat. Phys. **7**, 412 (2011).
[8] D. J. Clarke, J. D. Sau, and S. Tewari, Majorana fermion exchange in quasi-one-dimensional networks, Phys. Rev. B **84**, 035120 (2011).
[9] B. I. Halperin, Y. Oreg, A. Stern, G. Refael, J. Alicea, and F. von Oppen, Adiabatic manipulations of Majorana fermions in a three-dimensional network of quantum wires, Phys. Rev. B **85**, 144501 (2012).
[10] M. Sekania, S. Plugge, M. Greiter, R. Thomale, and P. Schmitteckert, Braiding errors in interacting Majorana quantum wires, Phys. Rev. B **96**, 094307 (2017).
[11] K. Flensberg, Non-Abelian Operations on Majorana Fermions via Single-Charge Control, Phys. Rev. Lett. **106**, 090503 (2011).
[12] J. D. Sau, D. J. Clarke, and S. Tewari, Controlling non-Abelian statistics of Majorana fermions in semiconductor nanowires, Phys. Rev. B **84**, 094505 (2011).
[13] B. van Heck, A. R. Akhmerov, F. Hassler, M. Burrello, and C. Beenakker, Coulomb-assisted braiding of Majorana fermions in a Josephson junction array, New J. Phys. **14**, 035019 (2012).
[14] C. S. Amorim, K. Ebihara, A. Yamakage, Y. Tanaka, and M. Sato, Majorana braiding dynamics in nanowires, Phys. Rev. B **91**, 174305 (2015).
[15] T. Karzig, F. Pientka, G. Refael, and F. von Oppen, Shortcuts to non-Abelian braiding, Phys. Rev. B **91**, 201102(R) (2015).
[16] T. Karzig, Y. Oreg, G. Refael, and M. H. Freedman, Universal Geometric Path to a Robust Majorana Magic Gate, Phys. Rev. X **6**, 031019 (2016).
[17] C. Knapp, M. Zaletel, D. E. Liu, M. Cheng, P. Bonderson, and C. Nayak, The Nature and Correction of Diabatic Errors in Anyon Braiding, Phys. Rev. X **6**, 041003 (2016).
[18] S. Das Sarma, A. Nag, and J. D. Sau, How to infer non-Abelian statistics and topological visibility from tunneling conductance properties of realistic Majorana nanowires, Phys. Rev. B **94**, 035143 (2016).
[19] D. J. Clarke, J. D. Sau, and S. Das Sarma, Probability and braiding statistics in Majorana nanowires, Phys. Rev. B **95**, 155451 (2017).
[20] C. Malciu, L. Mazza, and C. Mora, Braiding Majorana zero modes using quantum dots, Phys. Rev. B **98**, 165426 (2018).
[21] J. Liu, W. Q. Chen, M. Gong, Y. J. Wu, and X. C. Xie, Minimal setup for non-Abelian braiding of Majorana zero modes, Sci. China: Phys., Mech. Astron. **64**, 117811 (2021).
[22] P. Bonderson, M. Freedman, and C. Nayak, Measurement-Only Topological Quantum Computation, Phys. Rev. Lett. **101**, 010501 (2008).

[23] S. Hoffman, C. Schrade, J. Klinovaja, and D. Loss, Universal quantum computation with hybrid spin-Majorana qubits, Phys. Rev. B **94**, 045316 (2016).

[24] T. Karzig, C. Knapp, R. M. Lutchyn, P. Bonderson, M. B. Hastings, C. Nayak, J. Alicea, K. Flensberg, S. Plugge, Y. Oreg, C. M. Marcus, and M. H. Freedman, Scalable designs for quasiparticle-poisoning-protected topological quantum computation with Majorana zero modes, Phys. Rev. B **95**, 235305 (2017).

[25] S. Vijay and L. Fu, Teleportation-based quantum information processing with Majorana zero modes, Phys. Rev. B **94**, 235446 (2016).

[26] V. Kornich, X. Huang, E. Repin, and Y. V. Nazarov, Braiding and All Quantum Operations with Majorana Modes in 1D, Phys. Rev. Lett. **126**, 117701 (2021).

[27] B. Bauer, T. Karzig, R. V. Mishmash, A. E. Antipov, and J. Alicea, Dynamics of Majorana-based qubits operated with an array of tunable gates, Sci. Post Phys. **5**, 004 (2018).

[28] F. Harper, A. Pushp, and R. Roy, Majorana braiding in realistic nanowire Y-junctions and tuning forks, Phys. Rev. Research **1**, 033207 (2019).

[29] A. Conlon, D. Pellegrino, J. K. Slingerland, S. Dooley, and G. Kells, Error generation and propagation in Majorana-based topological qubits, Phys. Rev. B **100**, 134307 (2019).

[30] C. Tutschku, R. W. Reinthaler, C. Lei, A. H. MacDonald, and E. M. Hankiewicz, Majorana-based quantum computing in nanowire devices, Phys. Rev. B **102**, 125407 (2020).

[31] Marek Narożniak, M. C. Dartiailh, J. P. Dowling, J. Shabani, and T. Byrnes, Quantum gates for Majoranas zero modes in topological superconductors in one-dimensional geometry, Phys. Rev. B **103**, 205429 (2021).

[32] M. Cheng, V. Galitski, and S. Das Sarma, Nonadiabatic effects in the braiding of non-Abelian anyons in topological superconductors, Phys. Rev. B **84**, 104529 (2011).

[33] T. Karzig, G. Refael, and F. von Oppen, Boosting Majorana Zero Modes, Phys. Rev. X **3**, 041017 (2013).

[34] M. S. Scheurer and A. Shnirman, Nonadiabatic processes in Majorana qubit systems, Phys. Rev. B **88**, 064515 (2013).

[35] T. Karzig, A. Rahmani, F. von Oppen, and G. Refael, Optimal control of Majorana zero modes, Phys. Rev. B **91**, 201404(R) (2015).

[36] A. Rahmani, B. Seradjeh, and M. Franz, Optimal diabatic dynamics of Majorana-based quantum gates, Phys. Rev. B **96**, 075158 (2017).

[37] A. Nag and J. D. Sau, Diabatic errors in Majorana braiding with bosonic bath, Phys. Rev. B **100**, 014511 (2019).

[38] S. Gurvitz, Josephson-type effect in resonant-tunneling heterostructures, Phys. Rev. B **44**, 11924 (1991).

[39] F. Li, X. Q. Li, W. M. Zhang, and S. A. Gurvitz, Magnetic field switching in parallel quantum dots, Europhys. Lett. **88**, 37001 (2009).

[40] Y. S. Cao, L. T. Xu, J. Y. Meng, and X. Q. Li, Non-Markovian transmission through two quantum dots connected by a continuum, Phys. Lett. A **376**, 2989 (2012).

[41] S. Gurvitz, A. Aharony, and O. Entin-Wohlman, Temporal evolution of resonant transmission under telegraph noise, Phys. Rev. B **94**, 075437 (2016).

[42] X. Q. Li and L. T. Xu, Nonlocality of Majorana zero modes and teleportation: Self-consistent treatment based on the Bogoliubov–de Gennes equation, Phys. Rev. B **101**, 205401 (2020).